Computational Engineering and Physical Modeling 5-4 (2022) 1-22

Contents lists available at CEPM

Computational Engineering and Physical Modeling

Journal homepage: www.jcepm.com

Adaptive Neuro-Fuzzy Inference System (ANFIS) Integrated with Genetic Algorithm to Optimize Piezoelectric Cantilever-Oscillator-Spring Energy Harvester: Verification with Closed-Form Solution

Alireza Babaei[1*], Johné Parker[2*], Paria Moshave[3]

1. Ph.D. in Mechanical Engineering, University of Kentucky, United States
2. Associate Professor, Faculty of Engineering, University of Kentucky, United States
3. Ph.D. Student, University of Kentucky, United States

Corresponding author: *alireza.babaei@uky.edu* (A.B.); *johne.parker@uky.edu* (J.P.)

https://doi.org/10.22115/CEPM.2023.375302.1227

ARTICLE INFO

Article history:
Received: 03 December 2022
Revised: 11 March 2023
Accepted: 20 April 2023

Keywords:
Piezoelectric vibration-based energy harvester (PVEH);
Effective frequency bandwidth;
Soft computing;
Optimization;
Resonance frequency;
Harvested voltage.

ABSTRACT

Piezoelectric vibration-based energy harvesters (PVEHs) are designed to convert mechanical energy into electric energy. Researchers deal with issues like inefficient amount of energy and frequency bandwidth. Optimizing and widening the PVEH can address the issues. As a modification to the dynamic magnification concept of conventional PVEH, a novel integrated oscillatory multisystem of cantilever-oscillator-spring is proposed. In this project maximizing the widened effective frequency bandwidth with respect to the oscillator mass and spring constant is the main goal. The closed-form voltage function obtained numerically-analytically is expensive in terms of computational time and cannot be used in the genetic optimization. In this regard, soft computing techniques is adopted. Utilizing adaptive-neuro-fuzzy-inference-system (ANFIS), a regressor model is designed to estimate voltage function evaluations in the genetic optimization, such fuzzy system is tuned with decent type and number of membership functions according to the root-mean-square-error criteria. Fuzzy inference system (FIS) is implemented using 64 and 49 fuzzy rules derived from Gaussian membership functions (MFs) and passed to the genetic algorithm initiating with 100 iterations and 30 populations. Using roulette wheel, tournament, and random selection methods, optimal values of the mass and stiffness ratios are found to yield the most widened frequency bandwidth. Findings reveal integration of the proposed oscillator-spring subsystem drastically reinforces utmost generated voltage. Furthermore, tuning parameters result the maximum widened frequency bandwidth which improves the harvester performance up to 3 times the conventional values.

How to cite this article: Babaei A, Parker J, Moshaver P. Adaptive neuro-fuzzy inference system (ANFIS) integrated with genetic algorithm to optimize piezoelectric cantilever-oscillator-spring energy harvester: Verification with closed-form solution. Comput Eng Phys Model 2022;5(4): 1–22. https://doi.org/10.22115/cepm.2023.375302.1227

1. Introduction

Scavenging electrical energy from mechanical vibrations has been a trending research topic in recent years. Mechanical vibration energy is ubiquitous, free and clean. Adopting a proper transduction mechanism, one can generate free electric energy from any resource in oscillation. Doing so has mainly two benefits: the financial outcomes and the environmental preservation. Such idea is specifically important for integration of energy harvester modules with internet of thing (IoT) devices, micro-electro-mechanical-system, wireless sensor networks (WSNs), and RFID system; to form self-powered electro-mechanical systems [1]. Deleting the requirement of battery is one of the attractive goals as the need for replacement, labor cost, and environmental waste will all be obviated. Thus, piezoelectric vibration-based energy harvesters (PVEH) as one of the common energy modules have been studied deeply in the past decade. Such investigation encompasses structural modeling and analysis, along with material improvement. However, most of the current research articles focus on the devising novel models and vibratory response improvement. This is arisen from the vitality of matching the resonance frequency with driving (excitation) frequency coming from the external source, otherwise the amount of the generated energy is insignificant even with slight deviations from the resonance frequency. Another incentive to develop dynamical analysis and modeling is because of the effective (operational) frequency bandwidth. Similar to the frequency match, PVEH are effective enough only if the operational frequency bandwidth is widened. Mostly, widening the bandwidth and matching the resonance frequency are accommodated coextensively. To address such issues, tuning mass integration has been studied with great benefits. Tuning mass attached at the tip end of the cantilever decreases the cantilever resonance frequency. This point is specifically important since the resonance frequency of energy harvester substrates are mostly inaccessible. This particularly happens with small-scale and meso-scale systems where due to the size reduction; vibration modes take place usually at high numbers. On the opposite side, it is mostly hard to have high frequency values coming from external sources. Thus, decreasing the resonance frequency of the substrate by means of tuning masses improves the efficacy. Dynamic magnifiers introduce another development due to the active inertia of the magnifiers. In such systems, the effective frequency bandwidth is also widened. Such widening remarkably reinforces the successful and meaningful application of PVEH [2–5]. Naseer et al. [6] conducted a research to analyze the PVEH undergoing the vortex phenomena, where vibrations is generated due to the vortex of fluidics. Nonlinear analysis of energy harvesters using the harmonic balance approach is reported by Zhou et al. [7]. Harmonic balance is mainly a semi-analytical method to study the nonlinear oscillations from dynamic and frequency response curve aspect. Fan et al. [8] devised magnetically attractive coupling and stoppers to develop the efficacy of PVEH exposed to low-frequency excitations. The importance of magnet mass and the gap between the cantilever and the magnets are highlighted. Such parameters as the optimal design factors are helpful to optimize the energy harvester. Staaf et al. [9] designed a sliding tuning mass mechanism to enhance the effective frequency bandwidth. They noticed functionality of such a system in wireless sensor networks particularly under random (stochastic) excitations. Asthana et al. [10] improved energy harvesters in terms of operational (effective) frequency bandwidth. They used finite element method for the structural analysis part.

One of the remarkable issues with conventional energy harvesters refers to the narrow operational bandwidth at the vicinity of the resonance frequency. This means that with slight deviations of the excitation (driving) frequency from the resonance frequency, the harnessed voltage (as well as the harnessed electrical power) is drastically reduced. This challenging point results in deficiency of the energy harvesters. To address such a deficit, dynamic magnifiers are proposed. In other words, to further optimize the performance of a piezoelectric vibration-based energy harvester (PVEH), dynamic magnifiers have been utilized widely. Zhang et al. [11] studied the PVEH with constituents of advanced composites considering nonlinearities resulted from restoring force effects and magnetic forces in the field. In this research essay, harmonic balance method is adopted to find the semi-analytical response of the energy harvester with elaborations on the frequency response curves. Aladwani et al. [4] proposed a new type of configuration including cantilever beams which enables us to dynamically magnify the amount of harvestable energy. In this model, the rigid clamp supports of a beam are replaced with translational and rotational springs, along with holding two inertias at the two ends. Aladwani et al. [12] and Tang and Wang [13] extended the mentioned model and reported the significant widened operational frequency bandwidth whenever the dynamic magnifiers are employed including the eccentricity effects. Tang and Wang [3] investigated the size effects of the dynamic magnifiers at the tip ends. They considered the eccentricities of the tuning masses placed at the two ends and found the optimal eccentricities. Jia and Seshia [14] reported the experimental setup to find the optimal tuning mass value against the mass of the cantilever. Numerical results are also verified and validated with experimental results. Dechant et al. [15] studied the application of tuning masses integrated with cantilever beam arrays to reinforce the scavenged voltage. Nonlinear energy harvester analysis under a rotating element is studied by Mei et al. [16]. There are more technical articles addressing optimizing the PVEHs [17–20]. Based on the state-of-the-art provided, further developments in the design of PVEH are still expected. In this response; in this paper, integration of mass-spring subsystem with cantilever energy harvester is modeled and studied. For the first time, elastic support modeled via a spring transmits the inertia effects of the oscillator mass to the cantilever's boundary conditions. Besides, the cantilever's governing equation of motion is coupled to the oscillatory equation of the oscillator. In a separate article, we have studied that the oscillator mass and the spring stiffness constant directly alter the vibratory response of the proposed multisystem energy harvester, where significant deviations in: resonance frequencies, mode shapes, and transmissibility are addressed. In this paper, we have extended the former research to study the impact of the subsystem integration (oscillator-spring) over the cantilever response in terms of harvested voltage. The ultimate goal is to widen the operational frequency bandwidth and optimize the system with respect to the oscillator mass and spring constant. In other words, it is essential to improve the vibratory response of energy harvesters to capture more energy, along with wider operational frequency bandwidth. Such items are deliverable by integrating a subsystem with the cantilever. Thus, analyzing the vibratory response of the mentioned multi-system is important to assess the energy harvester's performance improvement. Finally, for the first time, the proposed model is optimized with respect to the oscillator mass and spring stiffness to widen the effective frequency bandwidth, meaning that for which values of the mentioned parameters and for a given excitation, the bandwidth is the most widened bandwidth possible. This is specifically important to increase the

application of such energy harvesters due to covering wider bandwidth. Addressing the bandwidth issue can lead to increment of piezoelectric energy harvesters applications in low-power electronics as a power supply.

2. Mathematical modeling and kinematics

To obtain the governing system of equations, first one needs to define the displacement fields. The schematic configuration of the multi system of cantilever-oscillator-spring energy harvester is shown in the following picture:

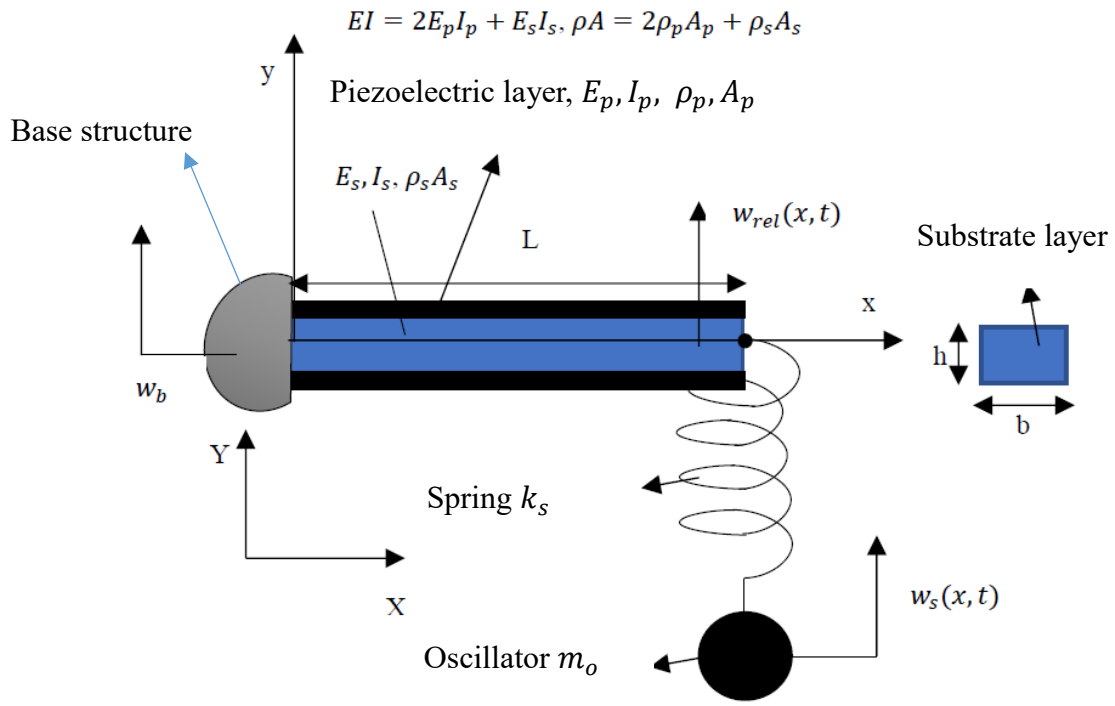

Fig. 1. Schematic of the cantilever-spring-mass energy harvester.

ρ_s, ρ_p are substrate and piezoelectric layers density, A_s, A_p show substrate and piezoelectric layers cross section areas, E_s, E_p represent substrate and piezoelectric layers Yung's modulus, I_s, I_p are substrate and piezoelectric layers second moment of inertia, beam has length of L, thickness of h, width of b; $x-y$ represents the Lagrangian cartesian coordinates, $X-Y$ is the fixed Eulerian cartesian coordinates. $w_b(x,t)$ is the base excitation, and $w_{rel}(x,t)$ and $w_s(t)$ represent relative lateral displacement of beam and oscillator with respect to the Lagrangian coordinates, respectively. According to the Euler-Bernoulli beam models; displacement fields are defined as follows:

$$u_x(x,z,t) = -y\frac{\partial w_{rel}}{\partial x}(x,t) \tag{1a}$$

$$u_y(x,z,t) = w_{rel}(x,t) \tag{1b}$$

$$u_z(x,z,t) = 0 \tag{1c}$$

To consider non-conservative work induced to the system, extended Hamilton's principle will be utilized. Based on plane-stress assumptions for liner isotropic elements following Hooke's law, constitutive relations of substrate and piezoelectric layers can be expressed as follows:

$$T_1{}^s = E_s S_1 \tag{2}$$

$T_1{}^s$ is stress, S_1 is strain of substrate layer. Based on the piezoelectric constitutive equations stress-strain and electric field relations are:

$$T_1{}^p = E_p(S_1 - d_{31}E_3) \tag{3a}$$

$$\varepsilon_{33}{}^s = \varepsilon_{33}{}^T - d_{31}{}^2 E_p \tag{3b}$$

$$D_3 = d_{31}T_1{}^p + \varepsilon_{33}{}^T E_3 \tag{3c}$$

$T_1{}^p$ is stress at piezoelectric layers. d_{31} is piezoelectric coupling coefficient. E_3 is electric field in y-direction. $\varepsilon_{33}{}^s$ and $\varepsilon_{33}{}^T$ represent permittivity at constant strain and stress. D_3 is electric displacement which acts only in z-difrection, respectively. Two types of damping mechanisms, internal and external are considered in this study. Internal damping is modeled as Kelvin-Voigt damping also named as strain-rate damping:

$$T_d = c_s \dot{S}_1 \tag{4}$$

T_d is stress due to strain-rate damping and c_s illustrates viscoelastic damping coefficient due to structural viscoelasticity. Dot sign indicates differentiation in temporal domain. Both internal and external damping satisfy proportional damping criteria.

For the proposed cantilever beam model, the kinetic energy (U_k) due to base excitations is:

$$U_k = \frac{1}{2}\int_0^L \rho A(\dot{w}_{rel}(x,t) + \dot{w}_b(x,t))^2\, dx + \frac{1}{2}m_o(\dot{w}_{rel}(L,t) + \dot{w}_b(L,t) + \dot{w}_s(t))^2 \tag{5}$$

Strain energy generated due to deflections (U_s) is comprised of energy of the substrate and energy of the piezoelectric layers integrated over volume fractions (V_s, V_p):

$$U_s = \delta U_{s-1} + \delta U_{s-2} = \frac{1}{2}\int_{V_s} T_1{}^s S_1 dV_s + \frac{1}{2}\int_{V_p} T_1{}^p S_1 dV_p = \frac{1}{2}\int_{V_s} E_s S_1{}^2 dV_s + \frac{1}{2}\int_{V_p} E_p(S_1{}^2 - S_1 d_{31}E_3)dV_p \tag{6}$$

Electrical energy (W_e) is:

$$W_e = \frac{1}{2}\int_{V_p} D_3 E_3 dV_p \tag{7}$$

Using following auxiliary relations, Eq. (7) can be written in the form of Eq. (12):

$$\mathrm{E_3} = -\mathrm{v(t)}\Big/(2\mathrm{h_p}) \tag{8}$$

$$\mathrm{D_3} = \mathrm{d_{31}E_pS_1} - \varepsilon_{33}{}^{\mathrm{s}}\frac{\mathrm{v(t)}}{2\mathrm{h_p}} \tag{9}$$

$$\mathrm{C_p} = \frac{\varepsilon_{33}{}^{\mathrm{S}}\mathrm{bL}}{\mathrm{h_p}} \tag{10}$$

$$v(t) = R_l \dot{q}_3(t) \tag{11}$$

$$W_e = \frac{1}{2}\int_{V_p} -d_{31}E_p z w_{rel,xx}\left(\frac{-v(t)}{2h_p}\right)dV_p + \frac{1}{2}\int_{V_p} \varepsilon_{33}{}^{s}\left(\frac{-v(t)}{2h_p}\right)^2 dV_p \tag{12}$$

In which $v(t)$ is the voltage across the resistive load and $q_3(t)$ is the electric charge.

External virtual work (W_{nc}) resulting from damping and dissipating resistive load of electrical circuit is:

$$W_{nc} = -\frac{d}{dt}\int_0^L \frac{1}{2} c_a \,(w_{rel} + w_b)^2 dx - \frac{d}{dt}\int_{V_s} \frac{1}{2} T_s S_1 \, dV_s - \frac{d}{dt}\left(\frac{1}{2} R_l {q_3}^2(t)\right) \tag{13}$$

Hamilton's approach is one of the mostly well-known variational methods to derive the equations of motion of continuous systems. Based on the Hamilton's variational principle, variations of systems' Lagrangian ($L = U_k - U_s - U_{th} + W_e + W_{nc}$) is zero in a short time interval ($\int_{t_1}^{t_2} \delta L dt = 0$). To apply such a concept, variations of energy terms are to be obtained:

$$\begin{aligned}&\delta U_k = \\ &\int_0^L \rho A \left(\dot{w}_{rel}(x,t) + \dot{w}_b(x,t)\right)\delta\dot{w}_{rel}(x,t)dx + m_o\left(\dot{w}_{rel}(L,t) + \dot{w}_b(L,t) + \dot{w}_s(t)\right)\delta\dot{w}_s(t) + \\ &\int_0^L m_o \left(\dot{w}_{rel}(x,t) + \dot{w}_b(x,t) + \dot{w}_s(t)\right)\delta(x-L)\delta\dot{w}_{rel}(x,t)dx\end{aligned} \tag{14}$$

$$\delta U_{s-1} = E_s I_s w_{rel,xx}\delta w_{rel,x}\Big|_0^L - E_s I_s w_{rel,xxx}\delta w_{rel}\Big|_0^L + \int_0^L E_s I_s w_{rel,xxxx}\,\delta w_{rel}dx \tag{15}$$

$$\begin{aligned}&\delta U_{s-2} = 2I_p E_p w_{rel,xx}\delta w_{rel,x}\Big|_0^L - 2E_p I_p w_{rel,xxx}\delta w_{rel}\Big|_0^L + \int_0^L 2E_p I_p w_{rel,xxxx}\,\delta w_{rel}dx + \\ &-Q_p E_p \frac{d_{31}}{2h_p} v(t)[H(x) - H(x-L)]\delta w_{rel,x}\Big|_0^L + Q_p E_p \frac{d_{31}}{2h_p} v(t)[\delta(x) - \delta(x-L)]\delta w_{rel}\Big|_0^L - \\ &\int_0^L Q_p E_p \frac{d_{31}}{2h_p} v(t)\left[\acute{\delta}(x) - \acute{\delta}(x-L)\right]\delta w_{rel}dx - \int_0^L Q_p E_p \frac{d_{31}}{2h_p} w_{rel,xx}\delta\dot{v}(t)dx\end{aligned} \tag{16}$$

$$\delta U_{ss} = k_s w_s \delta w_s \tag{17}$$

$$\begin{aligned}&\delta W_e = -Q_p E_p \frac{d_{31}}{2h_p} v(t)[H(x) - H(x-L)]\delta w_{rel,x}\Big|_0^L + Q_p E_p \frac{d_{31}}{2h_p} v(t)[\delta(x) - \delta(x- \\ &L)]\delta w_{rel}\Big|_0^L - \int_0^L Q_p E_p \frac{d_{31}}{2h_p} v(t)\left[\acute{\delta}(x) - \acute{\delta}(x-L)\right]\delta w_{rel}dx - \int_0^L Q_p E_p \frac{d_{31}}{2h_p} w_{rel,xx}\delta\dot{v}(t)dx + \\ &\int_{V_p} \varepsilon_{33}{}^{s} \frac{v(t)}{(2h_p)^2}\delta v(t)dV_p\end{aligned} \tag{18}$$

$$\delta W_{nc} = -\int_0^L c_a(\dot{w}_{rel} + \dot{w}_b)\delta w_{rel}dx - \int_0^L c_s I\,\dot{w}_{rel,xxxx}\delta w_{rel}dx - \frac{\dot{v}(t)}{R_l}\delta v \tag{19}$$

In the above-mentioned equations I_s, I_p are second moment of inertia of the substrate and the piezoelectric layers. $H(x)$ is Heaviside (unit step) function to model concentrated coverage of electrodes in x-direction. $\delta(x)$ is Dirac delta function. Q_p is the first moment of inertia of the

piezoelectric layers. c_a and c_a denote the viscous air damping and the structural strain rate (Kelvin-Voigt) damping coefficients.

$$I_s = \int_{A_s} z^2 dA_s = \frac{1}{12} b {h_s}^3 \tag{20}$$

$$Q_p = \int_{A_p} z dA_p = \frac{1}{2} b h_p (h_p + h_s) \tag{21}$$

$$I_p = \int_{A_p} z^2 dA_p = \frac{1}{3} b h_p ({h_p}^2 + \frac{3}{2} h_p h_s + \frac{3}{4} {h_s}^2) \tag{22}$$

$$EI = E_s I_s + 2 E_p I_p \tag{23}$$

EI is the total flexural rigidity (bending stiffness) of the cantilever beam in bending. After some mathematical operations, the system of coupled electromechanical partial integro-differential equations of the cantilever-oscillator-spring piezoelectric beam is derived:

$$\rho A \ddot{w}_{rel}(x,t) + EI w_{rel,xxxx}(x,t) + c_a \dot{w}_{rel}(x,t) + c_s I \dot{w}_{rel,xxxx}(x,t) - \Gamma_2 v(t)[\acute{\delta}(x) - \acute{\delta}(x-L)] = -\rho A \ddot{w}_b(x,t) - c_a \ddot{w}_b(x,t) - m_o \delta(x-L) \ddot{w}_b(t) \tag{24a}$$

$$\int_0^L \Gamma_2 \, \dot{w}_{rel,xx}(x,t) dx + \frac{C_p}{2} \dot{v}(t) = -\frac{v(t)}{R_l} \tag{24b}$$

$$m_o(\ddot{w}_{rel}(L,t) + \ddot{w}_s(t) + \ddot{w}_b(L,t)) + k_s w_s(t) = 0 \tag{24c}$$

Where, Γ_2 is:

$$\Gamma_2 = \frac{E_p Q_p d_{31}}{h_p} \tag{25}$$

Corresponding boundary conditions of the modeled system is:

$$w_{rel}(0,t) = 0 \tag{26a}$$

$$w_{rel,x}(0,t) = 0 \tag{26b}$$

$$w_{rel,xx}(L,t) = 0 \tag{26c}$$

$$EI w_{rel,xxx}(L,t) - m_o\big(\ddot{w}_{rel}(L,t) + \ddot{w}_s(t)\big) = 0 \tag{26d}$$

Analytical-numerical solution approach using Galerkin's modal decomposition method

To find the system response, it is required to first discretize the system into spatial and temporal domains. Based on the Galerkin's decomposition, relative motion of the distributed-parameter system can be expressed by converging expansion series of temporal and spatial functions:

$$w_{rel}(x,t) = \sum_{n=1}^{\infty} \phi_n(x) \, \eta_n(t) \tag{27}$$

$\phi_n(x)$ is the mass-normalized eigenfunction corresponding to the free vibration case and $\eta_n(t)$ is the modal coordinate of the system in nth vibration mode. To find the eigenfunctions and the eigenvalues, spatial part can be assumed as an exponential function $\eta_n(t) = e^{j\omega_n t}$. j is the unit imaginary number, ω_n is the resonance frequency of the system, and t is the time variable. The

undamped free vibration system is simply obtainable and the boundary conditions are identical to the main system:

$$\rho A\ddot{w}_{rel}(x,t) + EIw_{rel,xxxx}(x,t) = 0 \tag{28a}$$

$$m_o(\ddot{w}_{rel}(L,t) + \ddot{w}_s(t)) + k_s w_s(t) = 0 \tag{28b}$$

$$w_{rel}(0,t) = 0 \tag{29a}$$

$$w_{rel,x}(0,t) = 0 \tag{29b}$$

$$w_{rel,xx}(L,t) = 0 \tag{29c}$$

$$EIw_{rel,xxx}(L,t) - m_o\big(\ddot{w}_{rel}(L,t) + \ddot{w}_s(t)\big) = 0 \tag{29d}$$

General proposed solution for $\phi_n(x)$ is a linear combination of trigonometric and hyperbolic functions:

$$\phi_n(x) = \frac{1}{\sqrt{\rho AL}}\left(cosh\,\lambda_n x - cos\,\lambda_n x - \frac{cosh\,\lambda_n L + cos\,\lambda_n L}{sinh\,\lambda_n L + sin\,\lambda_n L}(sinh\,\lambda_n x - sin\,\lambda_n x)\right) \tag{30}$$

To further proceed, equation of the oscillator should be solved first.

$$\ddot{w}_s(t) + {\omega_{no}}^2 w_s(t) - {\omega_n}^2 \phi_n(L) e^{j\omega t} = 0 \tag{31}$$

Where ω_{no} represents the natural frequency of the oscillator ($\omega_{no} = \sqrt{k_s/m_o}$). Particular solution (transient response) for oscillations of the oscillator is:

$$w_s(t) = \frac{{\omega_n}^2}{{\omega_{no}}^2 - {\omega_n}^2}\phi_n(L) e^{j\omega t} \tag{32}$$

Applying the natural boundary conditions of a cantilever to Eq. (35a), the transcendental characteristic equation is derived with $\lambda_n L$ as the roots (eigenvalues):

$$\left(\frac{m_o L^3}{\rho AL}{\lambda_n}^4 - \frac{k_s L^3}{EIL}\right)(1 + cos(\lambda_n L)\,cosh(\lambda_n L)) - \lambda_n\left(\frac{m_o}{\rho AL}\right)\left(\frac{k_s L^3}{EI}\right)(sinh(\lambda_n L)\,cos(\lambda_n L) - cosh(\lambda_n L)\,sin(\lambda_n L)) = 0 \tag{33}$$

Introducing the mass ratio ($r_m = \frac{m_o}{\rho AL}$) and the stiffness ratio ($r_s = \frac{k_s}{(EI/L^3)}$) parameters, one can re-write the transcendental nonlinear characteristic equation in the following format:

$$r_s r_m(\lambda_n L)(sinh(\lambda_n L)\,cos(\lambda_n L) - cosh(\lambda_n L)\,sin(\lambda_n L)) - (r_s - r_m(\lambda_n L)^4)(1 + cos(\lambda_n L)\,cosh(\lambda_n L)) = 0 \tag{34}$$

The obtained equations is obviously different than the equation pertinent to the cantilever system ([21]). It is understandable that setting the mass and stiffness ratios equal to zero, yields the conventional characteristic equation. Eq. (40) is a transcendental and nonlinear equation which does not have a closed-form and exact solution. Consequently, numerical solvers are considered. Among numerical solver algorithms available, VPASOLVE is a decent solver included within MATLAB software package. However, similar to most of the numerical solvers, VPASOLVE

accuracy totally relies on the value of the initial guess. To better provide such initial guesses, plotting the equations sounds useful.

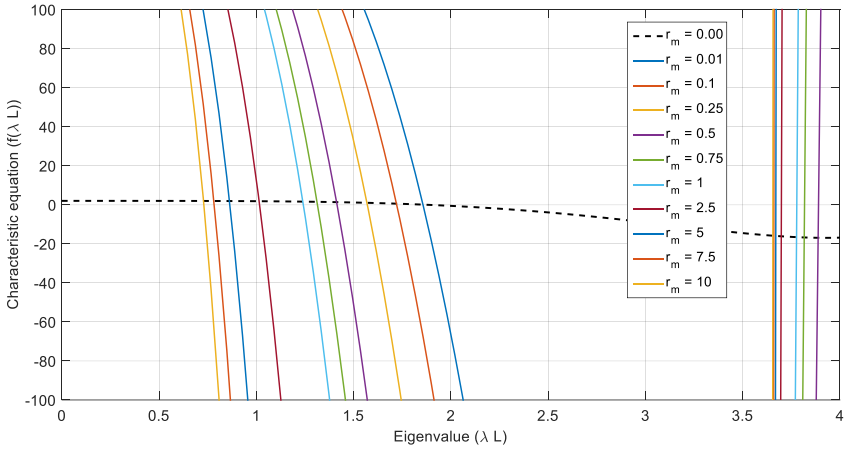

Fig. 2. Characteristic equation for different values of mass ratio and $r_s = 0.01$.

A comprehensive study about the vibratory and structural dynamics of cantilever-oscillator-spring system is accomplished in another technical essay, which conducts the numerical method to peruse frequency shifts due to the spring constant and oscillator mass. After finding the eigenvalues of the system, one can find the time and spatial-domain response using the Galerkin's approach. Substitution of Eq. (27) into Eq. (24a), multiplying both sides by $\phi_m(x)$ and integrating over the length of the beam along with benefiting the orthogonality of eigenfunctions, partial differential equation can be converted into time-domain ordinary differential equation:

$$\ddot{\eta}_n(t) + \left(\frac{c_s I}{EI}{\omega_n}^2 + \frac{c_a}{\rho A}\right)\dot{\eta}_n(t) + {\omega_n}^2\,\eta_n(t) = (\chi_n v(t) + (\rho A\gamma_n + m_o{\gamma_n}^o){\omega_e}^2 Y_0 e^{j\omega_e t})/B_n \quad (35)$$

Where,

$$B_n = \int_0^L \phi_{n,xx}(x)\phi_n(x)dx \quad (36a)$$

$$\gamma_n = \int_0^L \phi_n(x)dx \quad (36b)$$

$$\gamma_n = \phi_n(L) \quad (36c)$$

$$\chi_n = \Gamma_2 \phi_{n,x}\big|_L \quad (36d)$$

It is assumed the excitation to the system is harmonic ($w_b(t) = Y_0 e^{j\omega_e t}$). According to the linearity and principle of superposition, output voltage can also be assumed as a harmonic function unknown amplitude V_0:

$$v(t) = V_0 e^{j\omega_e t} \quad (37)$$

Substituting Eqs. (35) and (44) into Eq. (32) yields Eq. (45):

$$\dot{v}(t) + \frac{1}{\tau_c}v(t) = -\sum_{n=1}^{\infty}\Theta_n\,\dot{\eta}_n(t) \quad (38a)$$

$$\tau_c = \frac{C_p R_l}{2} \tag{38b}$$

$$\Theta_n = \frac{2\Gamma_2}{C_p}\phi_{n,x}\big|_L \tag{38c}$$

In energy harvesting systems, steady-state response of the vibratory part is of primary concern. Thus, particular answer part of the Eq. (35) is to be obtained:

$$\eta_n(t) = \frac{(\rho A\gamma_n + m_o{\gamma_n}^o)Y_0{\omega_e}^2 + \chi_n V_0}{B_n({\omega_n}^2 - {\omega_e}^2 + j2\zeta_n\omega_n\omega_e)} e^{j\omega_e t} \tag{39}$$

In Eq. (39), ζ_n is modal damping term:

$$\zeta_n = \frac{c_a}{2\rho A\omega_n} + \frac{c_s I}{2EI}\omega_n \tag{40}$$

Now, substitution Eq. (39) into Eq. (38a) results the output voltage across the resistive load:

$$v(t) = \frac{\sum_{n=1}^{\infty} \frac{-j\Theta_n(\rho A\gamma_n + m_o{\gamma_n}^o){\omega_e}^3 Y_0}{B_n({\omega_n}^2 - {\omega_e}^2 + j2\zeta_n\omega_n\omega_e)}}{\frac{1}{\tau_c} + j\omega_e + \sum_{n=1}^{\infty} \frac{j\Theta_n\chi_n\omega_e}{B_n({\omega_n}^2 - {\omega_e}^2 + j2\zeta_n\omega_n\omega_e)}} e^{j\omega_e t} \tag{41}$$

Besides to the output voltage, shunted vibration response of the cantilever can be found as follows:

$$w_{rel}(x,t) = \sum_{n=1}^{\infty} \frac{1}{\sqrt{\rho AL}} \left(\cosh\lambda_n x - \cos\lambda_n x - \frac{\cosh\lambda_n L + \cos\lambda_n L}{\sinh\lambda_n L + \sin\lambda_n L}(\sinh\lambda_n x - \sin\lambda_n x)\right) \frac{(\rho A\gamma_n + m_o{\gamma_n}^o)Y_0{\omega_e}^2 + \chi_n \frac{\sum_{n=1}^{\infty} \frac{-j\Theta_n(\rho A\gamma_n + m_o{\gamma_n}^o)\gamma_n{\omega_e}^3}{B_n({\omega_n}^2 - {\omega_e}^2 + j2\zeta_n\omega_n\omega_e)}}{\frac{1}{\tau_c} + j\omega_e + \sum_{n=1}^{\infty} \frac{j\Theta_n\chi_n\omega_e}{B_n({\omega_n}^2 - {\omega_e}^2 + j2\zeta_n\omega_n\omega_e)}}}{B_n({\omega_n}^2 - {\omega_e}^2 + j2\zeta_n\omega_n\omega_e)} e^{j\omega_e t} \tag{42}$$

Results and discussion

To study and optimize the operational frequency bandwidth, steady-state response of the system is of concern. Properties of the harvester piezoelectric beam are presented in the following Table.

Table 1
Geometric and mechanical properties of beam [22].

Beam length	$\boldsymbol{L = 100mm}$
Beam width	$b = 20mm$
Substrate layer thickness	$h_s = 5\mu m$
PZT layer thickness	$h_p = 4\mu m$
PZT modulus of elasticity	$E_p = 66\ GPa$
PZT mass density	$\rho = 7800\frac{kg}{m^3}$
PZT coupling coefficient	$d_{31} = -190\frac{pm}{V}$
PZT permittivity at constant strain	${\varepsilon_{33}}^s = 15.93\frac{nF}{m}$
electric circuit resistance	$R_l = 10^6\Omega$

Similar to the continuous (distributed-parameter) systems, the first few vibration modes are of major interest. This concept is valid for analyzing the effective frequency bandwidth as the most amount of extractable energy takes place in the initial modes. So, the excitation (driving) frequency is supposed to cover mostly the initial resonances. Damping ratio of the cantilever is considered as following values which are obtained experimentally [22]:

Table 2
Proportional damping values for first three modes of vibration [22].

ζ_1	ζ_1	ζ_1
0.010	0.013	0.033

2.1. Output electric frequency response functions (V-FRF, P-FRF)

Mostly, in coupled electromechanical systems voltage FRF (V-FRF) is defined as the modulus of the output voltage to the base acceleration induced to the harvester substrate.

$$\frac{v(t)}{\ddot{g}(t)} = \frac{\sum_{n=1}^{\infty} \frac{-j\Theta_n(\rho A\gamma_n + m_O\gamma_n{}^O)\omega_e}{B_n(\omega_n{}^2 - \omega_e{}^2 + j2\zeta_n\omega_n\omega_e)}}{\frac{1}{\tau_c} + j\omega_e + \sum_{n=1}^{\infty} \frac{j\Theta_n\chi_n\omega_e}{B_n(\omega_n{}^2 - \omega_e{}^2 + j2\zeta_n\omega_n\omega_e)}} \tag{43}$$

Accessing the voltage function, the power frequency response function (P-FRF) is simply obtainable similarly:

$$\frac{p(t)}{\ddot{g}(t)} = \left(\frac{\sum_{n=1}^{\infty} \frac{-j\Theta_n(\rho A\gamma_n + m_O\gamma_n{}^O)\omega_e}{B_n(\omega_n{}^2 - \omega_e{}^2 + j2\zeta_n\omega_n\omega_e)}}{\frac{1}{\tau_c} + j\omega_e + \sum_{n=1}^{\infty} \frac{j\Theta_n\chi_n\omega_e}{B_n(\omega_n{}^2 - \omega_e{}^2 + j2\zeta_n\omega_n\omega_e)}}\right)^2 / R_l \tag{44}$$

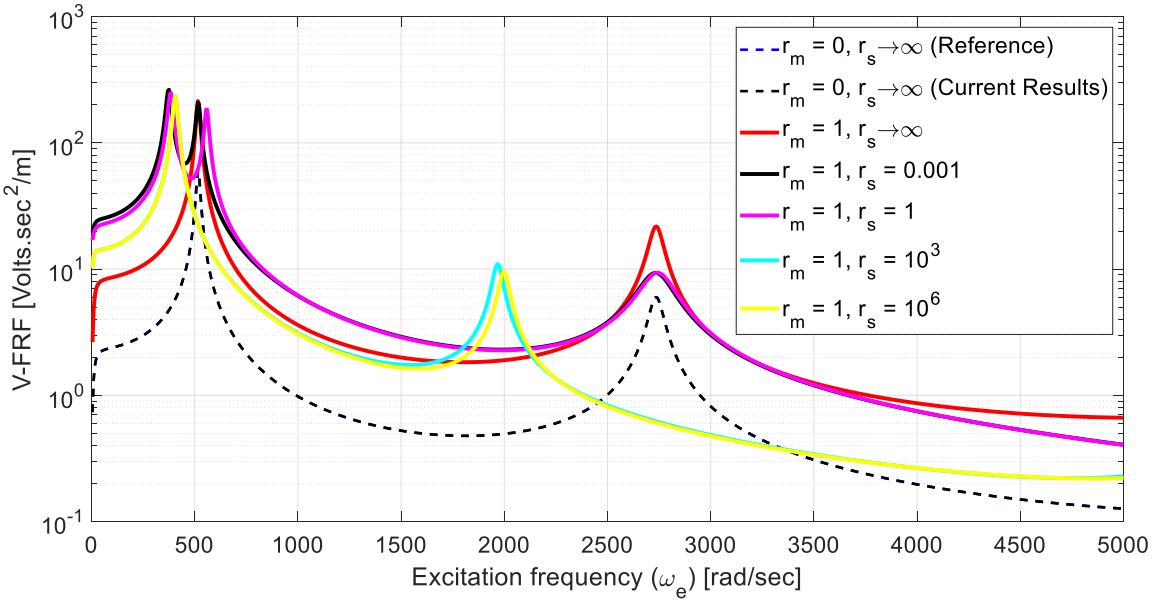

Fig. 3. Voltage frequency response function with respect to excitation frequency (constant mass ratio).

It is observed that for several values of the oscillator mass and spring constant, a minimal resonance takes place at the small numbers. This resonance is usually close to the second resonance. Based on this figure, it is observable that the integration of spring-mass subsystem with the cantilever notably improves the harvester's performance in terms of the amount of

harvestable energy as well as the effective frequency bandwidth. For example, the magenta line with an oscillator and stiffness ratios of 1 has wider bandwidth than the pure cantilever system shown in dashed blue line. It is also noteworthy that setting zero values for oscillator mass and soring stiffness (dashed black line) results in conventional pure cantilever. This line is verified against the reference ([22]) to validate current results.

2.2. Optimizing the cantilever-spring-oscillator energy harvester using soft computing

The effective frequency bandwidth is assumed as the difference between the minimal and the third resonances. As mentioned earlier, the ultimate goal is to find the specific values of oscillator mass and spring constant in which, the effective frequency bandwidth is the most widened bandwidth. Obviously, this is an optimization problem with the oscillator mass and spring constant as design parameters to be tuned. Such tuned parameters will optimize the effective frequency bandwidth as the objective (utility/fitness) function. To this end, the global algorithm of genetic optimization is taken. Genetic algorithm (GA) basically iterates for large number of times over the candidate solution and then over the evolutionary-generated solution populations. On the other hand, the derived voltage frequency response function (FRF) via analytical-numerical method, is a computationally-expensive function. It means that, it takes high level of computational time to evaluate the mentioned functions. This is mainly due to the large number of parameters in voltage FRF and the complexity of the function in nature. More importantly, the first step in using the analytical-numerical closed-form function is to find the eigenvalues of the nonlinear transcendental characteristic equation which needs to be repeated per each oscillator mass and spring constant values. Keeping in mind that the mentioned characteristic equation is solved by numerical methods (e.g., VPASOLVE), decent initial guess is demanded which requires plotting the function. There is not a consolidated computer program script to get the mass and stiffness ratios and generate the voltage FRF subsequently. This means that eigenvalue and voltage function evaluations are both hard-to-evaluate and non-automatic processes. Considering both the curse of time computations and manual process; evaluation of the both functions is impossible for high number of iterations. To obviate such a problem, soft computing algorithms including: fuzzy logic, neural networks, and genetic optimization; can be adopted. As for the function evaluations, a regressor (function approximator) model is required. Such regressor model can be designed by training finite number of results with mass and stiffness ratios as the inputs and the resonance frequencies as the outputs. To train such prediction models, fuzzy logic is preferred to the other cases since it is established based on semantic descriptions which is interpretable. Besides, fuzzy logic is easier to train and works well with nonlinearity and imprecisions. Thus, fuzzy logic is a decent approach to train the regressor model to be used in the genetic algorithm.

This figure shows the outline of FIS in MATLAB using the ANFIS toolbox. In training decent fuzzy logic architecture, type and number of membership functions (MFs), scales and range of the membership functions are determined and tuned. Such tuning can be improved with the adoption of neural networks where the learning capability is added to the fuzzy inference system (FIS). Thus adaptive-neuro-fuzzy-inference-system (ANFIS) in MATLAB is used.

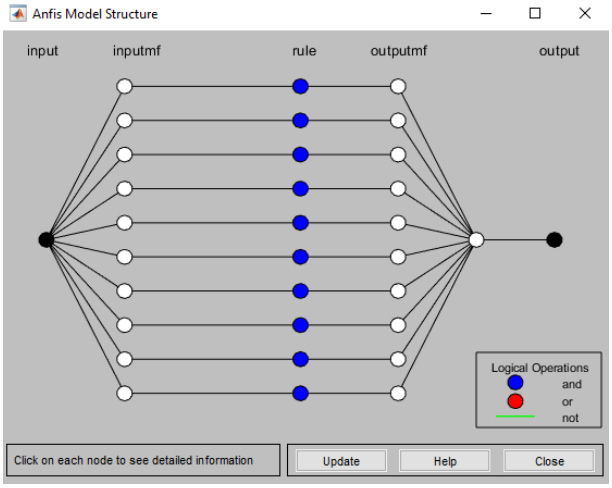

Fig. 4. Adaptive neuro fuzzy inference system structure.

2.3. Designing adaptive-neuro-fuzzy-inference-system (ANFIS)

To train the fuzzy inference system to learn the pattern of the voltage function, 231 cases (11 different values for $r_m = [10^{-4}, 10^{6}]$ and 21 different values for $r_s = [10^{-4}, 10^{2}]$) have been perused using the analytical-numerical closed-form expression of the voltage FRF to obtain the dataset.

The generated voltage dataset of is divided into train set (80%), validation (checking) set (10%), and test set (10%). Test dataset is used to evaluate the performance of the trained model on the new and unseen data. On the other hand, validation (checking) dataset is created to avoid overfitting of the model. It is also good to note that overfitting and underfitting mainly pertains to the complexity of the model. If the model is too simple, it will fail to predict even with the train dataset, this is known as the underfitting issue. Such models are computationally fast but practically lack precision. Increasing the complexity of the model leads to more accurate predictions. However, this will also result in more computational time. Besides to the computational cost issue, highly complex models perform well with the train dataset but fail to generalize and operate correctly with the new unseen datasets in terms of accuracy and precision. This is known as the overfitting issue which means the model fails to generalize. Similarly, such too complex models are not desired. To avoid the overfitting issue by means of cross validation technique, ANFIS toolbox in MATLAB is equipped with checking (validation) dataset. To train a decent fuzzy inference system (FIS), eight different membership function types are tested for the estimation of first frequency. Same procedure is duplicated for the third resonance. As for increasing the FIS capability, the raw dataset is preprocessed by taking the logarithm to the base of 10.

Table 3
ANFIS training properties for first and third resonances.

Number of MF for $\boldsymbol{r_m}$: 7, 8	Neural network optimization: Hybrid	Fuzzy type: Takagi Sugeno (MISO)
Number of MF for $\boldsymbol{r_s}$: 7, 8	Number of Epochs: 300	Number of Fuzzy rules: 49, 64
Type of MF: Gaussian	Error tolerance: 0	
FIS Generation: Grid partitioning	Output MF type: Constant	

In the above table, brief information about the generated FISs is listed which are used to compare and choose the best type of MFs.

Table 4
Different types of MFs (300 Epochs and 7 by 7 MFs) for first (minimal) resonance.

MF type	Train error	Test error	Validation error
Triangular	0.0068735	0.13659	0.096411
trapezoidal	0.010127	0.13489	0.10126
Bell	0.0069811	0.13598	0.092355
Gaussian	0.0068203	0.13632	0.092211
Gauss2	0.0094394	0.13704	0.098782
Polynomial	0.037733	0.12612	0.11003
Polynomial-sigmoid	0.0011285	0.14043	0.09739
Double sigmoid	0.011307	0.14044	0.097398

Complicated and nonlinear MF usually start with better initial guesses. While, the simple and linear MF (e.g., trapezoid and triangular) usually initiate with weak kickoffs and as a result require more epochs and computational efforts. According to the different root-mean-square-error (RMSE) for train, test and validation datasets; it is evident that Gauss, polynomial, trapezoidal, and bell type of membership functions show the best performance in capturing the structure of the dataset and ending in the least test error. The value of RMSE for test dataset looks more important in adopting the proper MF, other RMSE values (RMSE for train and validation datasets) can be handy in cases where the test RMSE values are close to each other. Gauss MF looks the best function with the best RMSE values for overall train, test, and validation dataset root-mean-square-errors (RMSEs).

Table 5
Different types of MFs (300 Epochs and 7 by 7 MFs) for third resonance.

MF type	Train error	Test error	Validation error
Triangular	0.0097362	0.16244	0.031308
Trapezoidal	0.012658	0.16402	0.024406
Bell	0.0085471	0.15886	0.022625
Gauss	0.008666	0.15791	0.018515
Gauss2	0.0088859	0.16234	0.014357
Polynomial	0.014318	0.16453	0.025687
Polynomial-sigmoid	0.0088589	0.16211	0.014197
Double-sigmoid	0.00888698	0.16211	0.014218

Similar assessment process is accomplished to choose the best operational membership function (MF) for training the neural networks and fuzzy inference sets corresponding to the third resonance frequency. In the above table, 8 different types of the built-in membership functions (MFs) are trained in two sets of 7 by 7 membership functions for each case and 300 epochs. By comparison, bell, and Gauss MFs reveal the smallest RMSE corresponding to the test dataset. Taking advantage of the RMSE for train and validation datasets, Gauss MF looks as the best MF with least root-mean-square-error overall. So, for both the first and the third resonances, Gaussian type of MFs are chosen.

Table 6
Comparison of different numbers of Gauss MF for the first resonance (300 epochs).

Number of MFs	Number of FIS rules	Train RMSE error	Test RMS error	Validation RMSE error
4 by 4	16	0.020586	0.13979	0.098779
5 by 5	25	0.012186	0.14225	0.13314
6 by 6	36	0.0051999	0.14459	0.11353
7 by 7	49	0.0068761	0.13632	0.092211
8 by 8	64	0.0030542	0.14326	0.088407
9 by 9	81	0.00313	0.42387	0.44046
10 by 10	100	0.0005196	0.18506	0.38915
11 by 11	121	0.00043178	0.27641	0.61551

After choosing the most accurate type of MF to train the fuzzy inference system; number of membership functions (MFs) per each input, and the corresponding number of generated fuzzy rules for the entire fuzzy inference system are to be determined. It is good to note, since the adaptive-neural-fuzzy-inference-system (ANFIS) is established based on the Takagi Sugeno inference system, it accepts only the MISO (multi input single output). As a result, two different types of neural networks systems are designed, one for the minimal (first) resonance prediction, and the other one for estimating the third resonance. Neural networks is designed for various numbers of the MFs revealing the corresponding RMSE for train, test, and validation datasets. 64-fuzzy-rule system looks the best one as it has the smallest overall RMSE values.

Table 7
Comparison of different numbers of Gauss MF for the third resonance (300 epochs).

Number of MFs	**Number of FIS rules**	**Train RMSE error**	**Test RMS error**	**Validation RMSE error**
4 by 4	16	0.028322	0.15453	0.032258
5 by 5	25	0.0314667	0.16453	0.027144
6 by 6	36	0.012834	0.15349	0.020544
7 by 7	49	0.008666	0.15791	0.018515
8 by 8	64	0.0084171	0.21796	0.16123
9 by 9	81	0.00042842	0.38683	0.30777
10 by 10	100	0.00045149	0.57157	1.0133
11 by 11	121	0.00025684	1.0601	1.0177

The above table is provided to compare different numbers of MFs and the corresponding generated fuzzy rules for the third resonance. Starting from a 5 by 5 fuzzy system and increasing up to 11 by 11 fuzzy system; the 49-fuzzy-rule system generated from a 7 by 7 system performs the most accurately due to the least overall train, test, and validation RMSE values.

Table 8
Frequency bandwidth between the first and the third resonance.

Frequency bandwidth	$r_s = 10^{-4}$	$r_s = 10^{-2}$	$r_s = 1$	$r_s = 10^{2}$
$r_s = 10^{-4}$	2.6396	2.4644	2.4789	2.4794
$r_s = 1$	4.0444	2.0485	2.3902	2.4798
$r_s = 10$	6.5456	3.3876	2.4322	2.6886
$r_s = 10^{6}$	6.5445	6.4426	5.5732	5.6069

In Table 8 different values of mass and stiffness ratios are chosen arbitrarily and the corresponding frequency bandwidth is calculated using Gaussian fuzzy inference system. It is good to note wider dataset is used in the fuzzy inference system and this table is shown as a sample.

Table 9
Sample of fuzzy rules used in ANFIS for the third resonance.

Rule	IF Input 1 is	AND IF Input 2 is	THEN Output is
1	In input1 MF1	In input2 MF1	In output MF1
9	In input1 MF2	In input2 MF1	In output MF9
20	In input1 MF3	In input2 MF4	In output MF20
30	In input1 MF4	In input2 MF6	In output MF30
45	In input1 MF6	In input2 MF5	In output MF45
64	In input1 MF1	In input2 MF1	In output MF64

Total of 64 rules are generated from the 8 by 8 fuzzy structure. The rules are connected with each other by 'and' connection method and with unit weight per rule. 6 rules are represented in the above table to show how IF-THEN rules in fuzzy inference system form a set of rules.

Table 10
ANFIS information for third resonance using Gaussian membership function.

ANFIS properties	
Fuzzy operations And-Method	Prod
Fuzzy operations Or-Method	Probor
Implication method	Prod (minimum)
Aggregation method	Sum (maximum)
Defuzzification method	wtaver
Input 1 membership function range	[-2,6]
Input 2 membership function range	[-2,4]
Output membership function range	[-1,2.6]
Connection type between the rules	And
Weight per each rule	1

Details about the type and structure of the ANFIS designed for the third resonance is presented in the above table.

Table 11
ANFIS information for third resonance using Gaussian membership function.

ANFIS properties	
Fuzzy operations And-Method	Prod
Fuzzy operations Or-Method	Probor
Implication method	Prod (minimum)
Aggregation method	Sum (maximum)
Defuzzification method	wtaver
Input 1 membership function range	[-2,6]
Input 2 membership function range	[-2,4]
Output membership function range	[3.4,3.84]
Connection type between the rules	And
Weight per each rule	1

Similar table is shown in the above to provide detailed information about the structure of the ANFIS designed for the first resonance.

2.4. Genetic algorithm

After designing the fuzzy inference regressor system by means of neural networks, the regressor can be fed into the genetic algorithm to yield the maximum effective (operational) frequency bandwidth between the minimal (first) resonance and the third resonance. This means, genetic optimization algorithm will find the optimal values of the mass and stiffness ratios (oscillator mass, and spring stiffness) so that the effective frequency bandwidth is widened the most for a given excitation. The reason for considering such a frequency bandwidth from the minimal resonance rather than the second resonance is due to the fact that such a minimal resonance does not take place in all of the design parameter values, and this way the impact of the new system configuration over the effective bandwidth is highlighted. Determining the design parameters range is a first step in optimization design problems. It is supposed for the spring constant to stay in the interval of $r_s = [0.01, 1]$ and the oscillator mass to fall in the interval of $r_s = [0.01, 2.5]$.

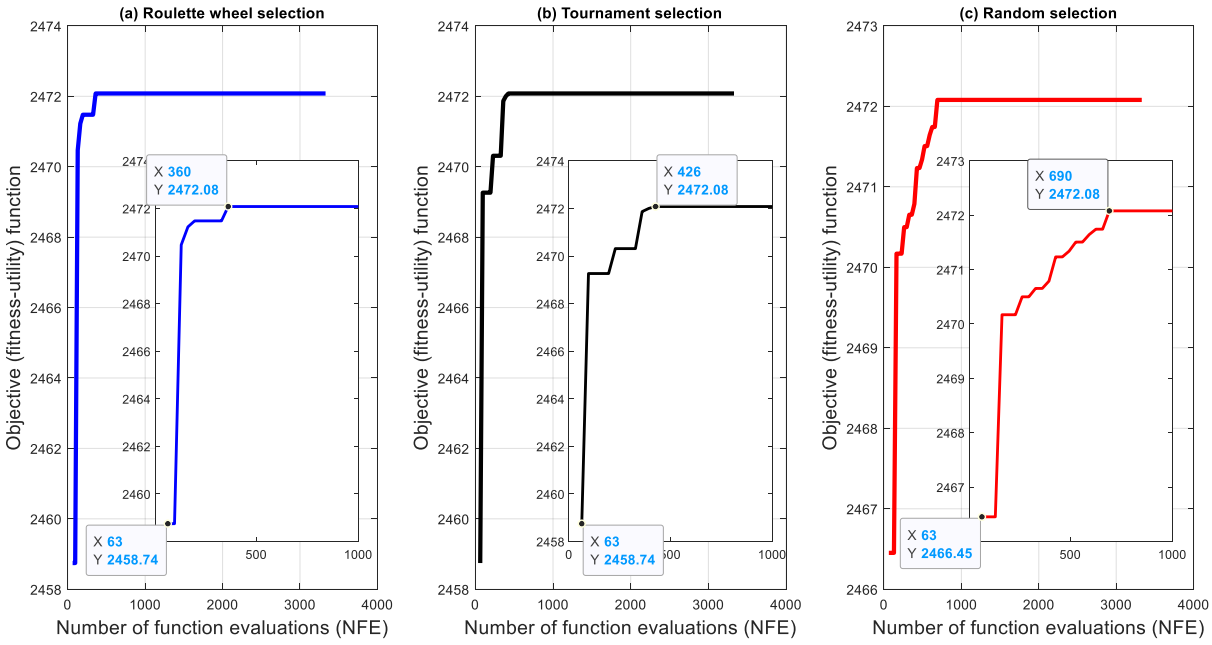

Fig. 9. Evolutionary path of the genetic optimization with different selections (Roulette wheel, tournoment, random).

This figure illustrates the genetic optimization evolutionary path throughout finding the optimal solution for the effective frequency bandwidth. Three different types of selection approaches (roulette wheel, tournament, and random) are applied within the genetic operations. Since the desired case is to widen the effective frequency bandwidth, the objective functions are indeed fitness or utility functions in terms of maximization problem.

Table 12
Summary of the genetic algorithm for optimizing the effective frequency bandwidth.

GA Selection type	Optimal r_m	Optimal r_s	Initial solution	Optimal solution	Total NFE
Roulette wheel	0.01	2.5	(63,2458.74)	(360,2472.08)	3330
Tournament	0.01	2.5	(63,2458.74)	(426, 2472.08)	3330
Random	0.01	2.5	(63,2466.45)	(690, 2472.08)	3330
Population	30				
Iteration	100				

Genetic algorithm properties of three different selection approaches are summarized in the above figure. According to the mentioned table and figure; optimal value for the oscillator mass is: $r_m = 2.5$ and that of the spring constant is: $r_s = 0.01$. the genetic algorithm is executed for 3330 number of function evaluations (NFEs). The algorithm initiated with 30 candidate solutions which also conveys the number of populations in each generation. The maximum number of iterations per each evolution is set to 100. Roulette wheel reaches the optimal solution in the least computational effort and is the most cost-effective selection method. Random selection initiates with a better initial solution but evolves through the longest computations comparatively. Tournament launches with the same initial guess as the roulette wheel but requires more computation time to find the optimal solutions. In short, the roulette wheel catches the optimal solution in the most cost-effective evolutionary path. As the final note, it is evident that roulette wheel shows more efficiency as it evolves with less genetic jumps (evolutions), tournament operates with medium genetic operational jumps and random traces a more complicated evolutionary track with several genetic operations. It is also good to note that since the nature of genetic algorithm is based on random initiation, disparate results in terms of cost-effectiveness of the evolutions may appear in next running efforts. After finding the optimal solution via soft computing algorithms, the soundness of the adopted technique is to be assessed. To do so, the optimal design parameter values will be taken for the analytical-numerical solution which is found as a closed-form expression in Eq. (43). So, for such optimal mass and stiffness ratios, the voltage frequency response function (FRF) is to be obtained and compared against several randomly-chosen case studies. Such a comparison is expected to certify the fact that the effective frequency bandwidth of the optimal solution is the most widened bandwidth. To find the voltage FRF, following steps are to be accomplished: using the nominated optimal values, one needs to plot the nonlinear transcendental characteristic equation to estimate the initial guesses. Such initial guesses will be utilized in the VPASOLVE algorithm to numerically solve the mentioned equation and to find the eigenvalues:

Table 13
Eigenvalues of the cantilever-oscillator-spring system using numerical method and for optimal case

r_s	r_m	$\lambda_1 L$	$\lambda_2 L$	$\lambda_3 L$
0.01	2.5	0.251277483823365	1.87661935315381	1.87661935315381

Next, the voltage FRF factors and the function values are found using the obtained eigenvalues.

2.5. Evaluation of the soft computing technique using analytical-numerical solution

The above figure depicts the voltage FRF for 9 case studies along with the reference case (pure cantilever, [22]). Oscillator mass and spring constants are chosen randomly. It is evident that the effective (operational) frequency bandwidth of the optimal solution is wider than any other cases shown in black line. In other words, this figure approves the authenticity and correctness of the ANFIS regressor system consolidated with the genetic algorithm in optimizing the bandwidth. Besides, findings reveal that the weak (soft) spring and the heavy oscillator contribute to the most widened energy harvester. This fact is observable in blue and yellow lines where the heavy oscillator inertia effects has widened the bandwidth via the soft spring. Current model is also verified against the benchmark in [22] showing high level of accuracy.

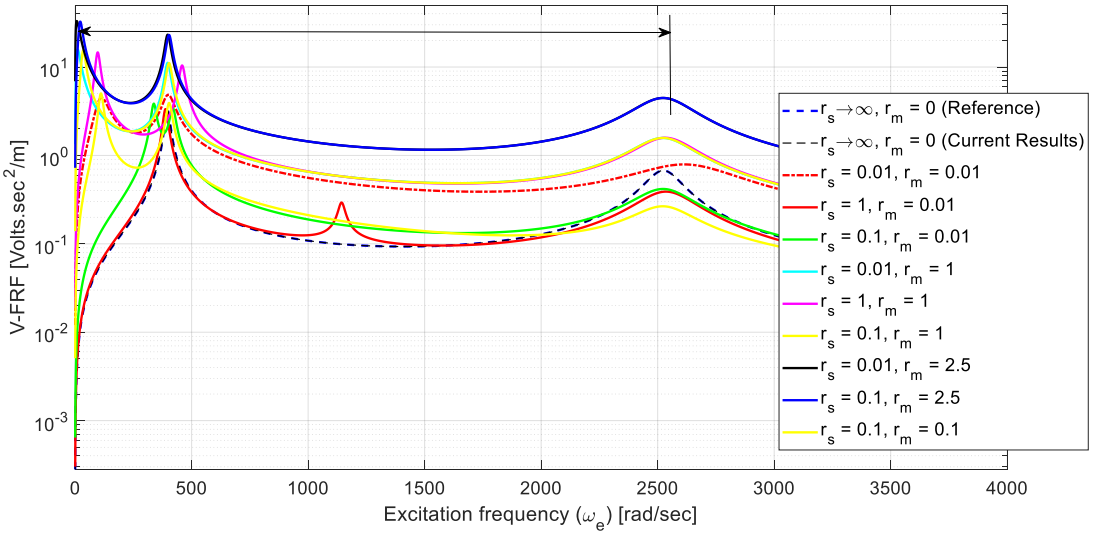

Fig. 10. Voltage FRF for different values of osccilator mass and spring constant values agasint the optimal value.

3. Discussion

Widening the effective or operational frequency bandwidth of piezoelectric vibration-based energy harvesters (PVEH) is vital as to cover more resonances and generate more electric power. Several approaches to maximize the effective frequency bandwidth has been proposed mostly based on the dynamic magnifier designs which is comprised of a tuning mass with rigid support and attached to the tip end of the cantilever. Considering the elastic support instead of the rigid support has never been studied before. In this paper, for the first time the attached mass is elastically connected to the cantilever via a spring. Such a subsystem of spring-oscillator renders the restoring force and inertia effects to the dynamic and electrical behavior of the cantilever. Such impact reinforces and develops the amount of harvested voltage as well as widening the operational frequency bandwidth. To take the most advantage of such a novel subsystem integration, values of the oscillator mass and spring stiffness are optimized to yield the most widened operational frequency bandwidth to harvest the maximum amount of electric energy from a given vibration energy. For the optimization, soft computing technique is used. The

proposed technique including: fuzzy logic, neural networks, and genetic optimization; is evaluated by analytical-numerical analysis. In the numerical-analytical section, extended Hamilton's principle is used to derive the electromechanical equations of: the beam, electric circuit, and oscillator. Due to the new type of integration and the subsequent new boundary condition, new resonance frequency is observed which can be adjusted by oscillator mass or spring constant. To optimize the energy harvester, bandwidth among the first and third resonances is considered as the effective frequency bandwidth and the objective (fitness/utility) function. Even though; closed-form expression for the voltage frequency response function (FRF) is analytically and numerically obtained, optimization algorithm requires a regressor model to estimate the utility function values per each iteration throughout the evolution. The reason for this is: the voltage function encompasses parameters that need to be found manually (i.e. guessing the initial guess to find the roots of the transcendental equation cannot be automated). Moreover, the mentioned function is computationally expensive. As a result, adaptive-neuro-fuzzy-inference-system (ANFIS) is utilized as a regressor to approximate the function values through genetic optimization. To train the neural network fuzzy regressor model, 231 cases are studied using the analytical-numerical voltage function. Since the Takagi-Sugeno fuzzy system as a multiple-input-single-output (MISO) is used in ANFIS, and the nature of current problem which requires two outputs, two separate fuzzy inference systems (FISs) are designed and tuned using neural networks for the first and third resonances. Proper type and number of the membership functions is developed using test dataset root-mean-square-error (RMSE) as the criteria which led to a 64 and 49 fuzzy rules based on the Gaussian membership functions. Such FIS models are used throughout the genetic algorithm initiating with random 30 candidate solutions and 100 iterations per evolution. Three different types of selection methods of roulette wheel, random, and tournament are used comparatively. All selection approaches yield identical optimal design parameter values ($r_s = 0.01, r_m = 2.5$). As for the verification of soft computing results, optimal voltage FRF is manually obtained using the analytical-numerical closed-form function and compared with 8 random cases of mass and stiffness ratio values. Furthermore, current model is also evaluated by comparing against the benchmark results. Comparison with random case studies proves the successful frequency bandwidth widening of the optimal case. Besides, the optimal case significantly reinforces the amount of harnessed voltage.

4. Conclusions

In this paper, new model for piezoelectric vibration-based energy harvester is studied to specifically analyze the importance of attaching an oscillator to the tip of the cantilever via elastic support. Such a novel design for energy harvesters is proposed to address the drawback with conventional energy harvesters in which the amount of harvestable energy is not enough, and the effective frequency bandwidth is very narrow. Considering the mass of the oscillator and stiffness of the spring, soft computing technique is developed to capture the optimal value of the oscillator mass and spring stiffness to render the optimized energy harvester. The optimal case not only is the most widened energy harvester but also improves the amount of maximum harvestable voltage showing notable improvements in the performance of the PVEHs. This paper

discloses successful integration of oscillatory subsystem with conventional cantilever energy harvesters to improve the amount of generated electric energy. Moreover, adjustable parameters of such subsystems can be tuned using soft computing techniques to optimize the effective frequency bandwidth to further develop the performance of PVEH. Final points of the this paper can be summarized in the following section:

Oscillator inertia and restoring forces of the spring, result in small resonance frequency which is very useful for low-frequency excitations

Attaching the oscillator using spring, improves the harvested amount of energy with a constant given excitation up to 300%.

Such improvement is extended into the widening of effective frequency bandwidth.

Such a model, has complicated characteristic equation which is hard to be evaluated in the genetic optimization algorithms with high evaluation numbers.

As a remedy, soft computing algorithms need to be developed to find the optimal values of oscillator mass and spring stiffness.

Developing the energy harvester model along with soft computing techniques, can lead to optimized piezoelectric vibration-based energy harvester to improve the performance by increasing the harvestable amount of voltage and widening the effective frequency bandwidth.

References

[1] Babaei A, Parker J, Moshaver P. Energy resource for a rfid system based on dynamic features of reddylevinson beam. ASME Int. Mech. Eng. Congr. Expo. Proc., vol. 7B-2020, 2020. https://doi.org/10.1115/IMECE2020-24174.

[2] Asthana P, Khanna G. Development of Vibration Piezoelectric Harvesters by the Optimum Design of Cantilever Structures. Nanogenerators, IntechOpen; 2020.

[3] Tang L, Wang J. Size effect of tip mass on performance of cantilevered piezoelectric energy harvester with a dynamic magnifier. Acta Mech 2017;228:3997–4015.

[4] Aladwani A, Arafa M, Aldraihem O, Baz A. Cantilevered piezoelectric energy harvester with a dynamic magnifier. J Vib Acoust 2012;134.

[5] Moon K, Choe J, Kim H, Ahn D, Jeong J. A method of broadening the bandwidth by tuning the proof mass in a piezoelectric energy harvesting cantilever. Sensors Actuators, A Phys 2018;276. https://doi.org/10.1016/j.sna.2018.04.004.

[6] Naseer R, Dai H, Abdelkefi A, Wang L. Comparative Study of Piezoelectric Vortex-Induced Vibration-Based Energy Harvesters with Multi-Stability Characteristics. Energies 2020;13:71.

[7] Zhou S, Cao J, Inman DJ, Lin J, Li D. Harmonic balance analysis of nonlinear tristable energy harvesters for performance enhancement. J Sound Vib 2016;373:223–35.

[8] Fan K, Tan Q, Liu H, Zhang Y, Cai M. Improved energy harvesting from low-frequency small vibrations through a monostable piezoelectric energy harvester. Mech Syst Signal Process 2019;117:594–608.

[9] Staaf LGH, Smith AD, Lundgren P, Folkow PD, Enoksson P. Effective piezoelectric energy harvesting with bandwidth enhancement by assymetry augmented self-tuning of conjoined cantilevers. Int J Mech Sci 2019;150. https://doi.org/10.1016/j.ijmecsci.2018.09.050.

[10] Asthana P, Dwivedi A, Khanna G. Finite Element Modeling of a Wideband Piezoelectric Energy Harvester for Ambient Vibration Extraction. Adv. VLSI, Commun. Signal Process., Springer; 2020, p. 549–56.

[11] Zhang X, Zuo M, Yang W, Wan X. A Tri-Stable Piezoelectric Vibration Energy Harvester for Composite Shape Beam: Nonlinear Modeling and Analysis. Sensors 2020;20:1370.

[12] Aladwani A, Aldraihem O, Baz A. A distributed parameter cantilevered piezoelectric energy harvester with a dynamic magnifier. Mech Adv Mater Struct 2014;21:566–78.

[13] Tang L, Wang J. Modeling and analysis of cantilever piezoelectric energy harvester with a new-type dynamic magnifier. Acta Mech 2018;229:4643–62.

[14] Jia Y, Seshia AA. Power Optimization by Mass Tuning for MEMS Piezoelectric Cantilever Vibration Energy Harvesting. J Microelectromechanical Syst 2016;25. https://doi.org/10.1109/JMEMS.2015.2496346.

[15] Dechant E, Fedulov F, Fetisov LY, Shamonin M. Bandwidth widening of piezoelectric cantilever beam arrays by mass-tip tuning for low-frequency vibration energy harvesting. Appl Sci 2017;7. https://doi.org/10.3390/app7121324.

[16] Mei X, Zhou S, Yang Z, Kaizuka T, Nakano K. A passively self-tuning nonlinear energy harvester in rotational motion: theoretical and experimental investigation. Smart Mater Struct 2020;29. https://doi.org/10.1088/1361-665X/ab78b2.

[17] Xu D, Hu Y, Chen H, Jia H, Liu P, Xin C. Fabrication and property of flexible macro fiber composites for vibration-based energy harvesting. Ceram Int 2023.

[18] Cai Q, Zhu S. The nexus between vibration-based energy harvesting and structural vibration control: A comprehensive review. Renew Sustain Energy Rev 2022;155:111920.

[19] Younis A, Dong Z, ElBadawy M, AlAnazi A, Salem H, AlAwadhi A. Design and Development of Bladeless Vibration-Based Piezoelectric Energy–Harvesting Wind Turbine. Appl Sci 2022;12:7769.

[20] Lan C, Qian F, Liao Y, Zuo L. Power characteristics of vibration-based piezoelectric energy harvesters: the effect of piezoelectric material nonlinearity. Smart Mater Struct 2022;31:105017. https://doi.org/10.1088/1361-665X/ac8efb.

[21] Meirovitch L. Fundamentals of vibrations. Waveland Press; 2010.

[22] Erturk A, Inman DJ. A distributed parameter electromechanical model for cantilevered piezoelectric energy harvesters. J Vib Acoust 2008;130.